Multiple Channels Mediate Calcium Leakage in the A7r5 Smooth Muscle-Derived Cell Line

Carlos A. Obejero-Paz, Stephen W. Jones, and Antonio Scarpa
Department of Physiology and Biophysics, Case Western Reserve University, Cleveland, Ohio 44106 USA

ABSTRACT Ca^{2+} entry under resting conditions may be important for contraction of vascular smooth muscle, but little is known about the mechanisms involved. Ca^{2+} leakage was studied in the A7r5 smooth muscle-derived cell line by patch-clamp techniques. Two channels that could mediate calcium influx at resting membrane potentials were characterized. In 110 mM Ba^{2+}, one channel had a slope conductance of 6.0 ± 0.6 pS and an extrapolated reversal potential of +41 ± 13 mV (mean ± SD, $n = 8$). The current rectified strongly, with no detectable outward current, even at +90 mV. Channel gating was voltage independent. A second type of channel had a linear current-voltage relationship, a slope conductance of 17.0 ± 3.2 pS, and a reversal potential of +7 ± 4 mV ($n = 9$). The open probability increased *e*-fold per 44 ± 10 mV depolarization ($n = 5$). Both channels were also observed in 110 mM Ca^{2+}. Noise analysis of whole-cell currents indicates that ~100 6-pS channels and 30 17-pS channels are open per cell. These 6-pS and 17-pS channels may contribute to resting calcium entry in vascular smooth muscle cells.

INTRODUCTION

The fine control of intracellular Ca^{2+} is key in the physiology of vascular smooth muscle cells. Different hormonal and physical stimuli modulate cytosolic calcium levels, and thus the contractile state, by adjusting the calcium entry and extrusion mechanisms (Orallo, 1996). One of the more conspicuous calcium entry mechanisms is the ill-defined "calcium leakage" (Loutzenhiser et al., 1984). In A7r5 cells, derived from embryonic rat aorta, the Ca^{2+} entry rate at rest is 0.06 fmol min^{-1} $cell^{-1}$ (Fayazi et al., 1996), corresponding to a whole-cell Ca^{2+} current of 0.2 pA $cell^{-1}$. Resting Ca^{2+} entry is comparable in intact smooth muscle (Van Breemen et al., 1986) and cultured smooth muscle cells from adult rat aorta (Orlov et al., 1993). Because of the small magnitude of these currents, and the lack of specific blockers, leak calcium pathways have not been investigated extensively or characterized in detail.

Experiments using ^{45}Ca show that most of the resting Ca^{2+} entry in vascular smooth muscle cells is insensitive to organic calcium channel blockers, but can be inhibited by Co^{2+}, Mn^{2+}, and lanthanides (Loutzenhiser et al., 1984; Orlov et al., 1993; Hayashi et al., 1991; Himpens et al., 1994). This suggests that additional pathways, distinct from L-type calcium channels, are involved. Indirect evidence from measurement of intracellular Ca^{2+} levels suggests that resting Ca^{2+} leakage in smooth muscle cells is a complex phenomenon involving multiple pathways for Ca^{2+}, Ba^{2+}, and Mn^{2+} entry (Hughes and Schachter, 1994), possibly due to the activity of more than one channel type. Ca^{2+}-permeable leak channels, with distinct gating and permeation characteristics, have been observed in several different cell types (Benham and Tsien, 1987; Coyne et al., 1987; Preston et al., 1992; Coulombe et al., 1989; Chesnoy-Marchais, 1985; Kuno et al., 1986; Franco and Lansman, 1990a; Rosenberg et al., 1988).

The physiological role of leak calcium entry in vascular smooth muscle cells is still speculative. Leakage channels could contribute to maintenance of the resting cytosolic Ca^{2+} level (Tsien and Tsien, 1990; Kargacin and Fay, 1991; Wong and Klassen, 1993). Leak calcium entry has also been suggested to be important for promoting Ca^{2+} oscillations (Goldbeter et al., 1990). Pathologically, leak Ca^{2+} entry, mediated through specific channels, is increased in Duchenne muscular dystrophy (Franco and Lansman, 1990a; Fong et al., 1990), and is probably responsible for the increased Ca^{2+} levels in diseased skeletal muscle.

The working hypothesis in this project was that calcium leakage in vascular smooth muscle cells results from the operation of specific channels that are open at resting membrane potentials. We have chosen the A7r5 cell line, derived from embryonic rat aorta (Kimes and Brandt, 1976), which has been extensively used as a model to investigate calcium homeostasis in vascular cells (Karaki et al., 1997). A7r5 cells express the same voltage-dependent and receptor-activated calcium channels observed in freshly isolated smooth muscle cells from rat aorta (Marks et al., 1990; Missiaen et al., 1990; Obejero-Paz et al., 1993; Byron and Taylor, 1995). Moreover, the kinetics of Ca^{2+} mobilization from the major Ca^{2+} sources (sarcoplasmic reticulum, mitochondria, and plasma membrane) is similar to differentiated smooth muscle cells (Lapidot et al., 1996). Given the small amount of calcium entry measured in ^{45}Ca experiments, we speculated that either few channels are open, the channel conductance for Ca^{2+} ions is small, or both. Using single-channel experiments, we found that resting Ca^{2+} influx is mediated by at least two different channel types that differ in gating kinetics and selectivity for Ca^{2+} ions.

Received for publication 2 January 1998 and in final form 11 June 1998.
Address reprint requests to Dr. Carlos A. Obejero-Paz, Department of Physiology and Biophysics, Case Western Reserve University School of Medicine, 10900 Euclid Ave., Cleveland, OH 44106. Tel.: 216-368-5519; Fax: 216-368-3952; E-mail: cao@po.cwru.edu.

0006-3495/98/09/1271/16 $2.00

To calculate the number of channels per cell, we compared power spectral densities from single-channel and whole-cell recordings. The results show that both channels are present at appropriately low densities. Preliminary reports of this work have been reported in abstract form (Obejero-Paz and Scarpa, 1992; Obejero-Paz et al., 1994, 1997, 1998).

MATERIALS AND METHODS

Cell preparation

The A7r5 cell line, derived from embryonic rat aorta, was obtained from the American Type Culture Collection (ATCC). Cells were grown as previously described (Marks et al., 1990). Before each experiment, confluent cell layers were dispersed with trypsin, resuspended in Dulbecco's modified Eagle's medium containing 0.5% fetal calf serum, and plated on Aclar slips. The medium contained 0.14 μg/ml cytochalasin D to maintain a rounded morphology and to improve seal formation (Marks et al., 1990). For the experiments described, the cells were placed in a 100-μl chamber that was continuously perfused at a rate of 5 ml/min. Experiments were carried out at room temperature (22 $\pm$ 2°C).

Single-channel experiments

The cell-attached configuration of the patch-clamp technique was used with an Axopatch-1B patch-clamp amplifier. Voltage commands were given and data were obtained using an AT-type computer, pClamp software (Clampex; Axon Instruments, Foster City, CA), and a Labmaster A-D converter. Current records were filtered at 1 kHz with a 4-pole Bessel filter and sampled at 5 kHz. Electrodes (~5 MΩ) were made with borosilicate glass (World Precision Instrument, New Haven, CT) and coated with silicone rubber. The standard pipette solution contained (in mM): 110 $BaCl_2$ or $CaCl_2$ and 10 HEPES. The pH was adjusted to 7.35 with NMG (*N*-methyl-D-glucamine). Seals were formed in a physiological salt solution containing (in mM) 150 NaCl, 2.5 Na-HEPES, 2 $CaCl_2$, pH 7.35, and the cell membrane potential was zeroed with a bath solution containing (in mM): 140 K-glutamate, 2 $MgCl_2$, 2 EGTA, and 10 NMG-HEPES, pH 7.35. This solution effectively zeroes the membrane potential, because potassium currents in cell-attached patches reversed at a value close to 0 mV with 140 mM KCl in the pipette (not shown). To minimize liquid junction potentials, the reference electrode was connected to the bath by means of a 3 M KCl agar bridge. No corrections were made for possible remaining junction potentials. The mean activity coefficients of the isotonic Ca^{2+} and Ba^{2+} solutions, calculated according to the method of Pitzer and Mayorga (1973), were 0.51 and 0.50, respectively. Using the Guggenheim convention (Shatkay, 1968), the activity coefficients for divalent cations and chloride ions in the extracellular (pipette) solution were 0.25 and 0.71, respectively. Because the solution bathing the cells contained low chloride, the intracellular chloride concentration was presumably lower than in the patch pipette, producing a negative reversal potential for chloride currents.

Single-channel analysis

Single-channel current amplitudes were calculated by fitting Gaussian functions to point-by-point amplitude histograms. Subconductance states were identified using mean-variance analysis (Patlak, 1993), calculating the variance in a seven-sample point window. Histograms included all points with a local variance below a criterion, which was varied to optimize separation of the peaks (see Fig. 1 *B*). To calculate the slope conductance, single-channel currents from individual experiments were plotted as a function of membrane potential and fitted to a straight line. The reversal potential from each experiment was calculated by extrapolation of the fitted line to zero current when currents did not reverse, or when currents were only recorded at negative membrane potentials. In experiments in which the reversal was directly observed, currents near reversal were fitted to a line, and the reversal potential was interpolated as the zero current level. Reversal potential (V_R) measurements were used to calculate the relative permeability (P) of channels to monovalent (M) and divalent (D) cations, assuming constant field theory (Lewis, 1979):

$$P_D/P_M = ([M]_i e^{V_R F/RT} - [M]_o)(1 + e^{-V_R F/RT})/(4[D]_o) \quad (1)$$

where F, R, and T have the usual meanings. Divalent (Ca^{2+} and Ba^{2+}) and monovalent (K^+) cation concentrations were converted to activities, multiplying by 0.25 and 0.74, respectively (Pitzer and Mayorga, 1973). Mg^{2+} was not included in the equation, because the intracellular Mg^{2+} concentration is relatively low (0.5 mM), and the contribution of this cation to outward currents should be negligible. In addition, we were unable to demonstrate Gd^{3+}-sensitive inward currents in 110 mM Mg^{2+} ($n = 2$). In fact, extracellular Mg^{2+} blocks resting Ba^{2+} currents (see Discussion).

For analysis of channel open and closed times, gating events were detected by half-amplitude threshold crossing analysis, for current records interpolated with eight points between every two sample points (Colquhoun and Sigworth, 1983). During the analysis, currents were filtered at 1 kHz with a Gaussian filter, so the effective cutoff frequency of the combined analog and digital filters was 700 Hz, with a rise time of 470 μs and a dead time of 250 μs (Colquhoun and Sigworth, 1983). Events longer than two dead times were used to construct open time and closed time histograms, which were plotted according to the method of Sigworth and Sine (1987). The maximum likelihood method was used to fit these histograms to the sum of exponential functions. We used twice the natural logarithm of the likelihood ratio to assess the number of exponential functions required to fit the distributions (Horn, 1987). The number of exponential functions was increased until the fitted distributions were not statistically different at the 5% level. Both fitted time constants (τ_i) and the fractions of events (a_i) were numbered starting from the shortest time constant.

The channels observed in this study gate in bursts. We defined bursts to include the two shortest closed time distributions, using the criterion of Jackson et al. (1983) to minimize the total number of misclassified events:

$$N_3 \exp(-t_c/\tau_3)/\tau_3 = N_2 \exp(-t_c/\tau_2)/\tau_2 \quad (2)$$

where t_c is the critical time, and N_i and τ_i are the fraction of events and time constant of the second and third exponential components of the closed time distribution. Mean burst lengths were calculated by fitting exponential functions to burst length distributions, or for small numbers of bursts, by averaging the burst lengths. To calculate the open probability in a burst, the sum of the open states within the burst was divided by the sum of open and closed states. NP_o values were obtained by dividing the number of sample points above the 50% threshold by the total number of samples in the record. The steady-state open probability (P_o) was calculated from records longer than 1 min by dividing NP_o by the number of channels (N). The number of channels per patch was estimated from the largest number of superimposed channel openings observed, which is a lower limit for the actual number of channels present.

Whole-cell experiments

Whole-cell currents were measured with the fast (classical) and perforated patch whole-cell configurations of the patch-clamp technique. Amphotericin B was used for the latter technique (Rae et al., 1991). Whole-cell calcium currents were recorded using the same isotonic Ba^{2+} solution used in single-channel experiments. The pipette solution used in the fast whole-cell configuration contained (in mM) 20 CsCl, 100 Cs glutamate, 0.5 $CaCl_2$, 5 $MgCl_2$, 12 EGTA, 10 HEPES, pH 7.35. The intracellular solutions contained either 1 mM Na_2GTP or 0.3 mM Na_2GTP and 5 mM Na_2ATP. The pipette solution for perforated patch clamp contained 75 $CsSO_4$, 55 CsCl, 5 $CaCl_2$, 10 HEPES, pH 7.35. Patch pipettes had resistances of 2–5 MΩ for classical whole cell and 1–2 MΩ for perforated patch. The access resistances were 3.8 $\pm$ 1.7 MΩ ($n = 21$) in classical whole cell and 6.0 $\pm$

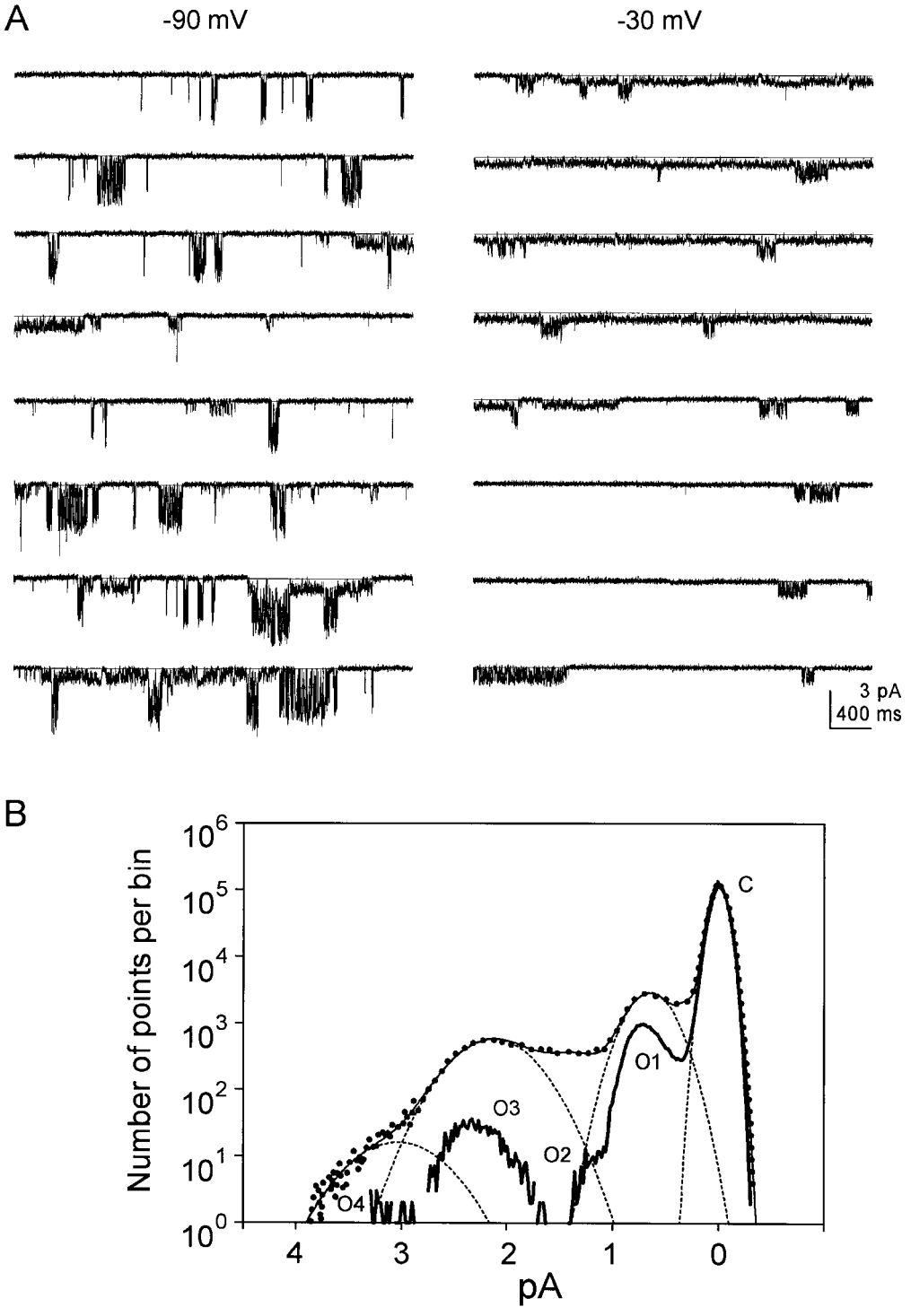

FIGURE 1 (*A*) Sample records of channel activity recorded in a cell attached patch at two voltages. Inward currents carried by 110 mM Ba^{2+} are in the downward direction. (*B*) Point-by-point amplitude histograms constructed from the record at −90 mV. Two histograms are shown superimposed, an all-point histogram (*dotted line*), and a histogram including only points with low local variance (*thick line*). The all-point histogram was fitted to the sum of six Gaussian functions with mean values (m_i), standard deviations, and fractions of the total number of data points (in parentheses) m_1 (labeled C in the figure) = 0.00 ± 0.07 pA (0.900), m_2 = −0.25 ± 0.11 pA (0.021), m_3 (labeled O1) = −0.65 ± 0.19 pA (0.051), m_4 = −1.32 ± 0.29 pA (0.010), m_5 (labeled O3) = −2.13 ± 0.32 pA (0.018), and m_6 (labeled O4) = −3.03 ± 0.37 pA (0.001). For clarity, Gaussian functions accounting for filtered transitions between the closed state and O1 (m2) and closed state and O3 (m4) were not shown.

1.4 MΩ (n = 7) in perforated patch. Whole-cell currents were filtered at 1 kHz with an 8-pole Bessel filter and sampled at 5 kHz. Resting Ba^{2+} currents were identified as the difference current present after blocking with 50 μM Gd^{3+}. Gd^{3+} was used because it effectively blocks leak calcium currents in skeletal muscle (Franco et al., 1991). Gd^{3+} was removed by washing for 45 s with solutions including 0.2 mM EGTA.

Noise analysis

The power spectral density of single-channel and whole-cell records was calculated using a fast Fourier transform routine (Press et al., 1992). Power spectra were averaged from at least 10 records lasting 3.27 s (16,384 sample points). For single-channel data, difference spectra were calculated as the average of spectra for records with channel activity, minus the averaged spectra for null records (records with no channel activity). For whole-cell currents, the spectrum of currents recorded in the presence of 50 μM Gd^{3+} was subtracted from the spectrum recorded without Gd^{3+}. The difference spectra were then analyzed between 0.3 Hz and 1000 Hz (single channels) or 500 Hz (whole cell). This was because whole-cell currents were also filtered by the combination of series resistance and membrane capacitance. In our experiments, using the classical whole-cell configuration, series resistance and capacitance were 4.8 ± 1.8 MΩ and 19.7 ± 3.8 pF (n = 7), respectively, producing an average effective cutoff frequency of 652 Hz (including the contribution of the 1 kHz analog filter).

The difference spectra were fitted to the sum of Lorentzian functions:

$$S(f) = \sum S_i(0)/(1 + (f/f_{ci})^2), \quad (3)$$

where $S_i(0)$ and f_{ci} are the zero frequency asymptote and corner frequency of each Lorentzian component. The number of Lorentzian functions that fit the power spectrum was increased until the fit was not significantly improved at the 0.05 level (Horn, 1987). The contribution of each Lorentzian component to the total noise was assessed by calculating the variance (σ^2_i):

$$\sigma_i^2 = S_i(0)\pi f_{ci}/2 \quad (4)$$

The time constant (τ_i) of each Lorentzian component was calculated from

$$\tau_i = 1/(2\pi f_{ci}). \quad (5)$$

Values were expressed as mean ± SD. Experimental results were compared using t-test statistics from Sigma Plot. Values less than 0.05 were considered statistically significant.

RESULTS

Single-channel experiments show that A7r5 cells express channels that permeate divalent cations at resting membrane potentials (Fig. 1 *A*). From inspection of the recordings, it is apparent that both large and small channels are present, each showing complex kinetic behavior. The point-by-point histogram calculated from the record at −90 mV, and drawn with the dotted line in Fig. 1 *B*, shows the presence of multiple current levels. Four major components were fitted to Gaussian functions, and the fitted lines are indicated with dashed lines. The fast gating of the large channel precluded a clear resolution of the different current levels. Thus mean variance analysis (see Materials and Methods) was used to exclude data points occurring during transitions. The histogram indicated with the thicker line in Fig. 1 *B* included only data points where the local variance was lower than 0.03 pA^2. Under these restricted conditions, four open levels can easily be identified. O1 and O3 are the main current levels, and O2 is an upper conductance level of the small channel (see below). During periods where both channels appeared to be active, a peak (O4) was observed at −3.0 pA, very close to the sum of the main conductance levels of the two channels (−2.8 pA). The additivity of current levels suggests the existence of two different channels, rather than subconductance states of a single channel. These two channels will be designated as 6-pS and 17-pS channels, according to their slope conductance in 110 mM Ba^{2+}.

6-pS channels with 110 mM Ba^{2+}

Selectivity for divalent cations and inward rectification

Fig. 1 *B* and the inset in Fig. 2 *A* show that 6-pS channels exhibit two current levels. Mean variance analysis from three patches showed that the amplitudes of the main (O1) and upper conductance levels at −60 mV were −0.54 ± 0.06 pA and −0.83 ± 0.08 pA, respectively. The open channel spent 98 ± 1% of the time in the major (6 pS) level and 2 ± 1% in the upper level (n = 3). The low frequency of the upper conductance level precluded further analysis. Thus the gating and permeation properties were characterized only for the more frequent conductance level. Fig. 2 shows current-voltage relationships for this component from channel records at different holding potentials (Fig. 2 *A*), or from voltage ramps between −90 and +90 mV (Fig. 2 *B*). From these experiments a slope conductance of 6.0 ± 0.6 pS (range 5.3–7.3) between −90 mV and 0 mV was calculated. Interestingly, 6-pS channels did not carry detectable outward currents, even at very positive potentials (Fig. 2 *B*). In the experiment shown in Fig. 2 *C*, channel rectification was investigated by changing the membrane potential between −60 mV and +60 mV during a long burst of channel activity. No detectable current was recorded at +60 mV, even when inward currents were immediately apparent during repolarization to −60 mV. Currents from this experiment were also plotted as triangles in Fig. 2 *B*, to show that the single-channel current shows comparable rectification whether measured from voltage ramps or from currents recorded at different holding potentials.

The reversal potential of this channel could not be measured directly, as outward currents were not observed. A lower limit for the reversal potential was determined by extrapolating the line fitted to the currents at negative membrane potentials to the zero current level. The extrapolated reversal potential from eight experiments was +41 ± 13 mV (range +26 to +60 mV). From Eq. 1, assuming that 140 mM K^+ is the main permeable intracellular ion, the permeability ratio P_{Ba}/P_K was 28, suggesting that 6-pS channels are selective for divalent over monovalent cations. A more positive reversal potential would yield an even larger P_{Ba}/P_K ratio.

Voltage-independent gating of 6-pS channels

In Fig. 3 *A*, NP_o values from four experiments are plotted as a function of the membrane potential. Within one patch, NP_o was not dependent on voltage. Differences in NP_o values across patches result, in part, from the presence of different number of channels in each patch. After correction for the estimated number of channels per patch, P_o from three experiments at −60 mV ranged from 0.10 to 0.68. This variability may be explained by the occasional pres-

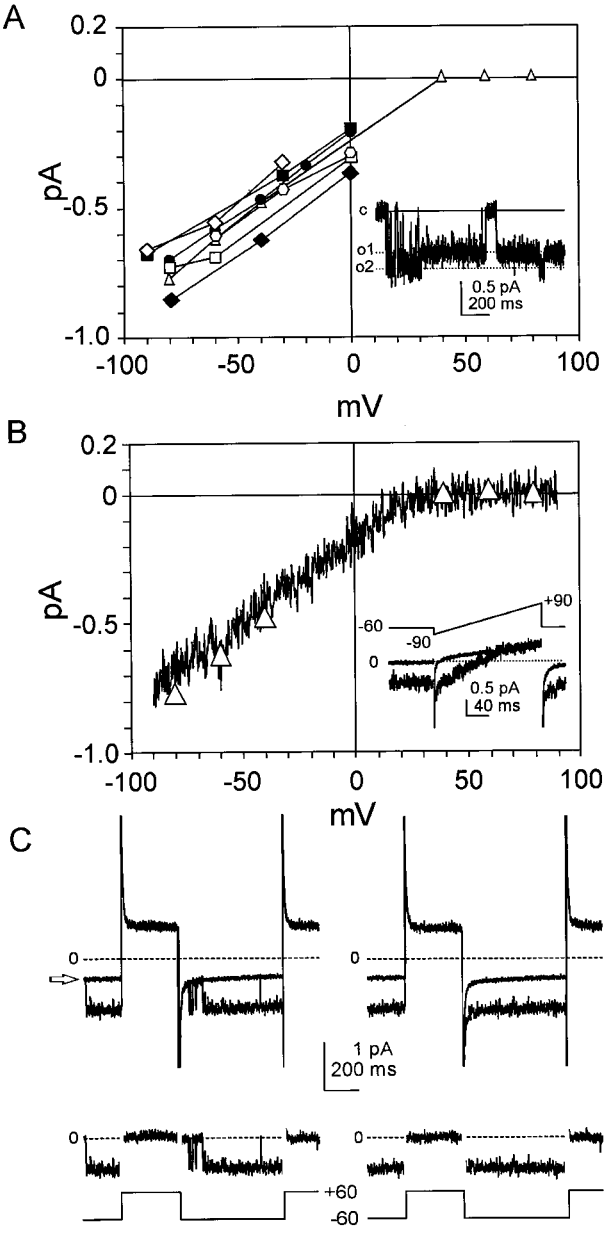

FIGURE 2 Current-voltage relationship of 6 pS channels. (*A*) Current-voltage relations measured from channel records at different holding potentials. Data points are the mean of two or more single-channel currents measured from the fit of Gaussian functions to point-by-point amplitude histograms. Each symbol represents a different patch. *Inset*: Single-channel record at −60 mV, showing the two conductance levels o1 and o2. (*B*) Inward rectification of the 6-pS channel demonstrated by a ramp protocol. Six sweeps were averaged, from a period where the channel was open immediately before and after a voltage ramp. The main panel shows leak-subtracted currents, using the average of seven ramps showing no channel activity. The inset show the voltage protocol, the current during a single sweep (*noisy record*, not leak subtracted), and the averaged leak current (*smooth record*). Patch 94o07. (*C*) Inward rectification of the 6-pS channel demonstrated by a step pulse protocol. *Top*: Raw data showing the leak current (*arrow*) and channel activity during the pulse protocol. The leak current is the average of three records showing no channel activity. *Bottom*: Difference current and pulse protocol. The membrane patch was held at −60 mV, with voltage steps to +60 mV at 1 Hz. For clarity, the artifact due to the capacitative transient was removed. Current amplitudes measured by this protocol are shown as open triangles in *A* and *B*. Patch c4o20.

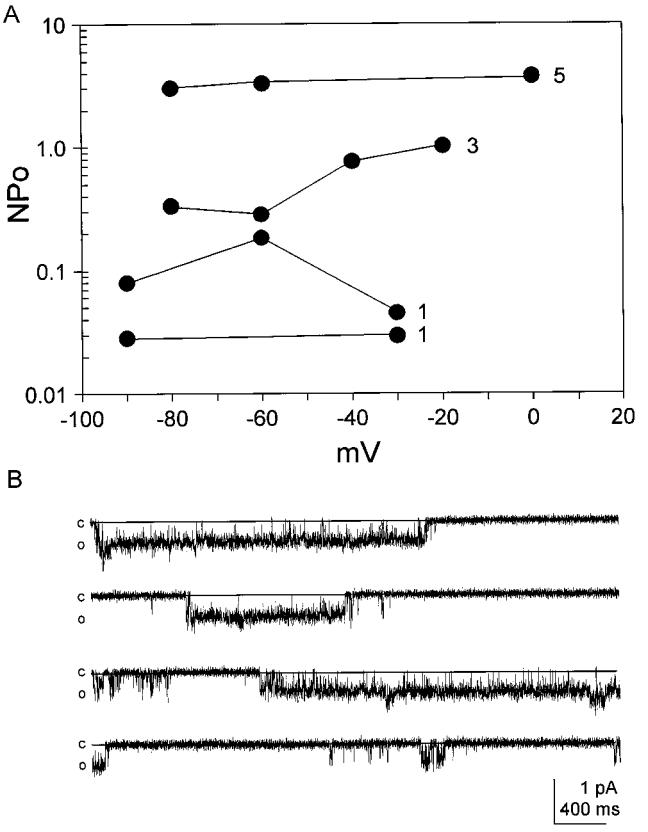

FIGURE 3 Voltage-independent gating of 6-pS channels. (*A*) NPo values from four experiments, calculated from records at least 1 min long at each membrane potential. The numbers at the right of each set of data points indicate the estimated number of channels in the patch. (*B*) Single-channel activity recorded at −60 mV, illustrating the heterogeneity of bursts. Patch 94o07.

ence of very long closed states, comparable to the length of the recording.

Six-pS channels show complex gating behavior, where openings may occur as single events or in bursts of different lengths (Fig. 3 *B*). Fig. 4 *A* shows that the open time distribution from four experiments between −90 and −60 mV could be fitted to three ($n = 2$) or four ($n = 2$) exponential functions, suggesting that the channel can access multiple open states. The fourth exponential component was required to fit a population of very long openings. The closed time distribution was also complex, fitted by the sum of four ($n = 2$) or five ($n = 2$) exponential functions (Fig. 4 *B*). The fifth exponential component accounted for a population of rare long closings, which occasionally lasted several minutes, so the parameters for that component may not have been estimated accurately. In addition, the shortest time constant was also difficult to assess, because it was only twice the dead time of the recording system (0.5 ms).

The voltage dependence of the open and closed events was assessed by comparing τ_i's and a_i's from two experiments between −90 and −30 mV, and −60 and −40 mV. In agreement with the voltage-independence of the steady-state open probability, no differences in time constants and

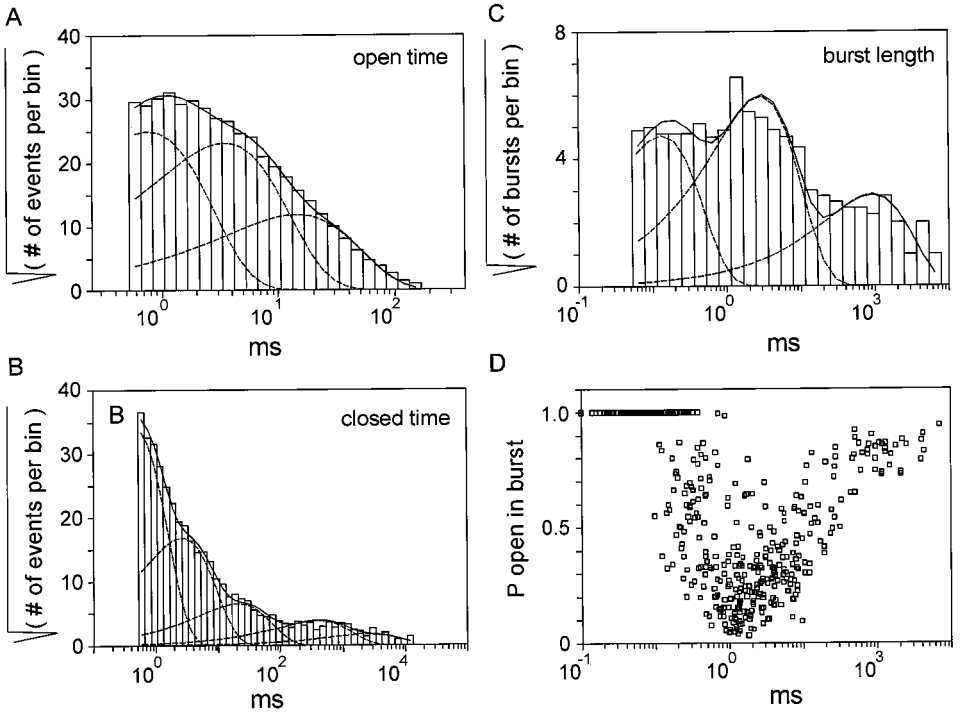

FIGURE 4 Complex gating of 6-pS channels. Open (*A*) and closed (*B*) time distributions were calculated from a 7-min record at −60 mV. The open time distribution was fitted to the sum of three exponential functions with time constants (τ_{Oi}) and fractions of open events (a_{Oi}): τ_{O1} = 0.8 ms, a_{O1} = 0.478; τ_{O2} = 3.5 ms, a_{O2} = 0.412; τ_{O3} = 14.4 ms, a_{O3} = 0.110. In four experiments, the open times were τ_{O1} = 0.8 ± 0.2 ms, a_{O1} = 0.43 ± 0.05; τ_{O2} = 4.1 ± 1.6 ms, a_{O2} = 0.35 ± 0.08; τ_{O3} = 18.2 ± 10.7 ms, a_{O3} = 0.17 ± 0.06; and τ_{O4} = 78 or 293 ms, a_{O4} = 0.06 or 0.10, in two patches. In this patch, the closed time distribution was fitted to the sum of five exponential functions: τ_{C1} = 0.4 ms, a_{C1} = 0.774; τ_{C2} = 2.7 ms, a_{C2} = 0.186; τ_{C3} = 20.8 ms, a_{C3} = 0.028; τ_{C4} = 394 ms, a_{C4} = 0.009; τ_{C5} = 2581 ms, a_{C5} = 0.002. In four experiments, the closed times were τ_{C1} = 0.4 ± 0.1 ms, a_{C1} = 0.74 ± 0.02; τ_{C2} = 2.1 ± 0.7 ms, a_{C2} = 0.18 ± 0.02; τ_{C3} = 12.5 ± 5.5 ms, a_{C3} = 0.06 ± 0.02; τ_{C4} = 216 ± 132 ms, a_{C4} = 0.02 ± 0.01; and τ_{C5} = 1.7 or 2.6 s, a_{C5} = 0.002 or 0.012. (*C*) The distribution of burst lengths. The critical closed time used to define a burst was 12.3 ms (Eq. 2). The burst length distribution was fitted to the sum of three exponential functions: τ_{B1} = 1.4 ms, a_{B1} = 0.339; τ_{B1} = 29.1 ms, a_{B1} = 0.537; τ_{B1} = 937 ms, a_{B1} = 0.125. In four patches, the mean values were τ_{B1} = 2.4 ± 1.3 ms, a_{B1} = 0.45 ± 0.09; τ_{B2} = 27 ± 9 ms, a_{B2} = 0.39 ± 0.09; and τ_{B3} = 464 ± 317 ms, a_{B3} = 0.16 ± 0.07. (*D*) Open probability during a burst, as a function of burst length. All data in this figure are from patch b3o01.

relative amplitudes were apparent in that range of membrane potentials (not shown). This suggests that the voltage-independent P_o reflects voltage-independent gating kinetics, not changes in opening and closing rates that may fortuitously cancel each other.

Fig. 3 *B* shows that 6-pS channels can open as single events, or in bursts of events of variable duration. Therefore it was important to investigate whether the different burst lengths represent distinct burst types, or are extremes within a single population of bursts. A burst was defined as a train of opening and closing events ending when a closure was longer than a critical time. This time was chosen to include the two shortest closed states within the burst (Eq. 2). Fig. 4 *C* shows the burst length distribution at −60 mV, fitted to three exponential functions.

Fig. 4 *D* shows the calculated P_o of each burst as a function of burst duration, using the same time scale as Fig. 4 *C* to allow direct comparison. The shortest bursts with P_o = 1 were, in fact, single isolated openings. Unexpectedly, the longest bursts were associated with higher P_o than the intermediate component, implying different gating kinetics within short and long bursts. The same pattern was observed at −30 mV (not shown), consistent with the voltage-independent kinetics of this channel.

Because τ_{C2} and τ_{C3} were relatively close, there was a significant possibility that individual closing events could be misclassified. To evaluate the effect of the critical time on the measured burst kinetics, the data were reanalyzed for shorter and longer times. These analyses also yielded three populations of bursts (including the single openings), with P_o higher for the longest component than for the intermediate component (not shown).

17 pS channels with 110 mM Ba^{2+}

Selectivity for divalent cations

Fig. 5 shows the current-voltage relationship from five experiments in which single-channel currents were measured from amplitude histograms. Currents through 17-pS channels show a linear relationship between −90 and +90 mV with slightly positive reversal potentials. The same linear relationship is shown in the inset, where the current was obtained from a voltage ramp between −90 and +90

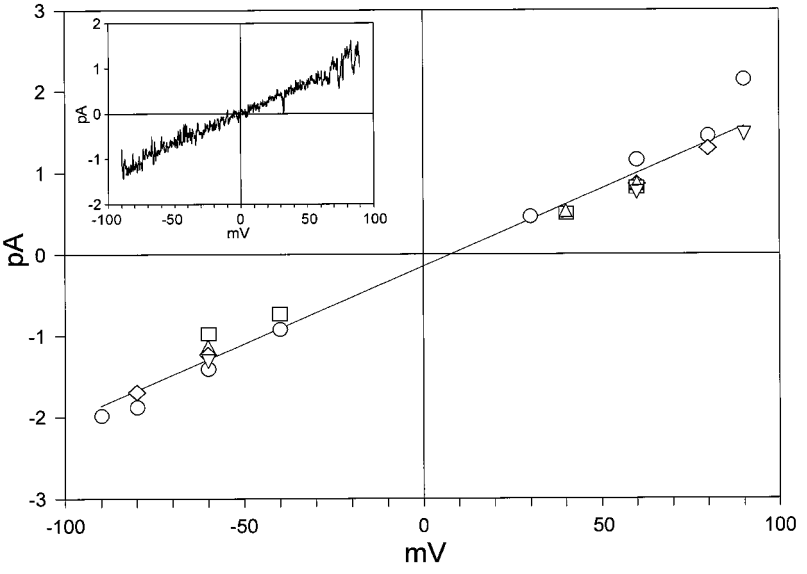

FIGURE 5 17-pS channels discriminate slightly between Ba^{2+} and K^+. The main panel is the current-voltage relationship obtained from five experiments represented with different symbols. The calculated slope conductance and reversal potential from the fit of the straight line were 19 pS and +8 mV, respectively. The inset shows a leak-subtracted current recorded during a voltage ramp between −90 mV and +90 mV. For leak subtraction, records without channel openings were averaged and fitted to multiple exponential functions. The fitted record was then subtracted from a ramp recorded during a burst of channel activity. Patch f4o08.

mV. Results from 10 experiments yield a slope conductance of 17.1 ± 3.2 pS, and a reversal potential of +7 ± 4 mV. For this reversal potential, the permeability ratio P_{Ba}/P_K was 2.9.

Voltage-dependent gating of 17-pS channels

The 17-pS channels exhibited complex, voltage-dependent gating (Fig. 6). P_o was higher at positive membrane potentials, shown either by voltage steps (Fig. 6 *A*) or by holding at different potentials for 1 min or more (Fig. 6 *B*). The net effect of depolarization was to increase P_o by *e*-fold for 44 ± 10 mV ($n = 5$) (Fig. 6 *B*).

One effect of depolarization was to evoke a population of long openings (Fig. 6 *A*). At −60 mV, the open time distribution was fitted to a single exponential function in four of five experiments, with a mean open time of 1.5 ± 0.7 ms (Fig. 7 *A*). At +60 mV, two exponential functions were required in four of five experiments, with $\tau_{O1} = 1.1 \pm 0.3$ ms and $\tau_{O2} = 10.4 \pm 3.0$ ms, and amplitudes $a_{O1} = 0.47 \pm 0.27$ and $a_{O2} = 0.66 \pm 0.05$ (Fig. 7 *A*). There was no detectable change in the open time constants with voltage (not shown).

The closed time distributions were complex, including components with time constants ranging from 1 ms to 2 s (not shown). Because the longer components were not always well defined, the gating of the 17-pS channel was further analyzed in terms of bursts (defined by Eq. 2; see Materials and Methods). At −60 mV, the distribution of burst lengths had two main components, corresponding to single openings ($\tau \approx 0.7$ ms) and to true bursts ($\tau = 52 \pm 39$ ms, $n = 9$) (Fig. 7 *B*). In three of nine experiments, the fit was improved statistically by the addition of an intermediate component with a time constant of 11.4 ± 6.2 ms. When present, this component accounted for 23 ± 7% of the bursts (range 4–21%). The longer burst duration increased with depolarization (Fig. 7 *B*). The intermediate and short burst durations showed no clear voltage dependence (not shown).

When analyzed in terms of bursts, there are three possible explanations for the observed increase in P_o with depolarization: an increased P_o during a burst, longer bursts, or shorter interburst closures. All three measures showed some degree of voltage dependence (Fig. 8). P_o during a burst was only weakly voltage-dependent (*e*-fold for 765 ± 551 mV), and was >0.5 at all voltages (Fig. 8 *A*), so this effect makes a relatively minor contribution to the overall dependence of P_o on voltage (>10-fold from −60 to +60 mV; Fig. 6 *B*). The length of the main (longest) burst duration component increased by *e*-fold for 83 ± 27 mV of depolarization (Fig. 8 *B*), resulting in part from a significant increase in the number of openings per burst (8 ± 4 at −60 mV, versus 14 ± 5 at +60 mV, $n = 5$). The distribution of closed times within a burst showed no clear voltage dependence (not shown). Because most patches analyzed contained more than one channel, and interburst closings tended to be few and long, the number of bursts per second was measured, rather than the distribution of interburst closed times (Fig. 8 *C*). The burst rate increased by *e*-fold per 94 ± 41 mV of depolarization. Taken together, these results imply that voltage must affect several rate constants in the kinetic scheme for gating of 17-pS channels, with the largest effects on the rates for entering and leaving a burst.

Evidence for two distinct channel populations

The evidence described above indicates the operation of two distinct classes of channels. This conclusion is consistent with a three-dimensional plot relating slope conductance, reversal potential, and mean burst duration (Fig. 9). The populations described above as 6-pS and 17-pS channels are encircled in the mV-pS plane by solid and dashed lines, respectively. The lower conductance channels had more

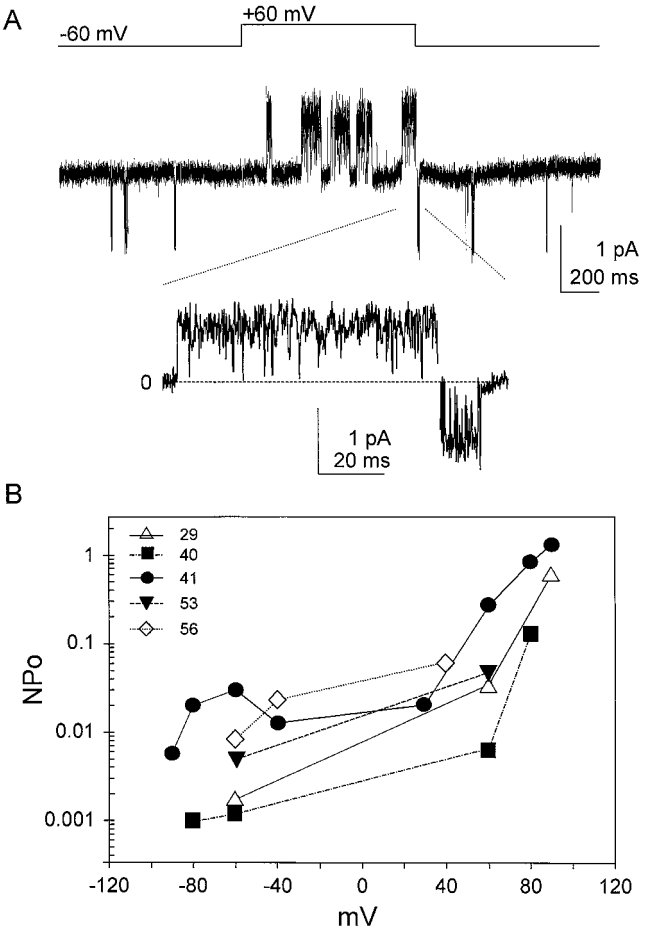

FIGURE 6 Voltage-dependent gating of 17-pS channels. (*A*) Channel activity recorded at −60 and +60 mV (*top*). Capacitive transients were fitted to two exponential functions and subtracted. Burst activity during the repolarization from +60 mV to −60 mV is shown in the bottom panel on an expanded time scale. Patch c5415. (*B*) NPo values from five experiments plotted as a function of membrane potential. Values were calculated from 1-min records. The number near each symbol is the change in voltage necessary to induce an *e*-fold increase in open probability, calculated by fitting a straight line to the experimental points.

positive reversal potentials and longer bursts. The detailed properties of the two classes of channel are summarized and compared in Table 1.

Only one observed channel, marked with an asterisk in Fig. 9, did not fit into this classification. This channel had a slope conductance of 15 pS, in the range of the large channels. However, all of the other parameters (a positive extrapolated reversal potential (+30 mV), the absence of outward current at positive membrane potentials, and voltage-independent gating at negative voltages) resembled those of the 6-pS channels (see Table 1).

Experiments using Ca^{2+} as current carrier

In cell-attached experiments using 110 mM Ca^{2+} as charge carrier, both large and small channels were observed, consistent with the two main classes of channel recorded in the presence of 110 mM Ba^{2+} (Fig. 10). Small channels, with even smaller single-channel current amplitudes than those observed in Ba^{2+} (−0.16 pA and −0.26 pA at −60 mV), were observed in 2 of 27 patches. In both experiments, a change in membrane potential from −80 mV to −60 mV had no detectable effect on single-channel currents, suggesting a low slope conductance. The small current precluded further analysis.

Large channels were recorded with Ca^{2+} in four patches. Whereas current amplitudes were comparable to those observed in Ba^{2+} (Fig. 10 *B*), large channels in Ca^{2+} showed a slightly smaller slope conductance ($p < 0.03$), with no significant difference in the extrapolated reversal potential. These parameters are compared in Table 1, along with channel gating properties. Replacing Ba^{2+} with Ca^{2+} did not affect the distribution of open and closed events within a burst, or the mean burst duration at negative membrane potentials. Moreover, NP_o values at −60 mV were similar, 0.010 ± 0.005 ($n = 3$) in Ca^{2+} and 0.009 ± 0.011 ($n = 5$) in Ba^{2+}.

Noise analysis of single-channel records

Noise analysis of single-channel records was used to further characterize the gating properties of 6-pS and 17-pS channels. This information will be used later to identify, in whole-cell currents, noise components due to the gating of these channels, and to count the number of channels. This is possible because, if channels gate independently, the power spectrum of a population of channels equals the power of a single channel multiplied by the total number of channels. As a corollary, the power spectra due to distinct types of channels are additive. Experiments were performed at −60 mV rather than a more depolarized membrane potential, to increase the single-channel amplitude and to avoid contamination with possible "window" T- or L-currents (see whole-cell data below).

Fig. 11 *A* shows the power spectral density of a 17-pS channel at −60 mV, calculated by subtracting the spectra shown in the inset. The power spectrum was well fitted by the sum of two Lorentzian functions depicted with dashed lines in Fig. 11 *A*. The corner frequencies from five experiments were 2.8 ± 0.5 Hz and 437 ± 35 Hz. Table 2 shows the corresponding time constants calculated from Eq. 5. The value of the longer component was similar to the mean burst duration (74 ± 38 ms) calculated from the same experiments. The approximation of the larger time constant to the mean burst duration is expected because bursts are infrequent, and closed times within the burst are short (see Colquhoun and Hawkes, 1995, for a theoretical justification). On the other hand, the kinetics of the fast Lorentzian component could not be clearly defined because the time constant was less than twice the dead time of the recording system (0.5 ms), and the noise approached the background noise levels (see *inset* in Fig. 11 *A*). From Eq. 4, 83% of the variance was due to the larger component. Thus the noise of

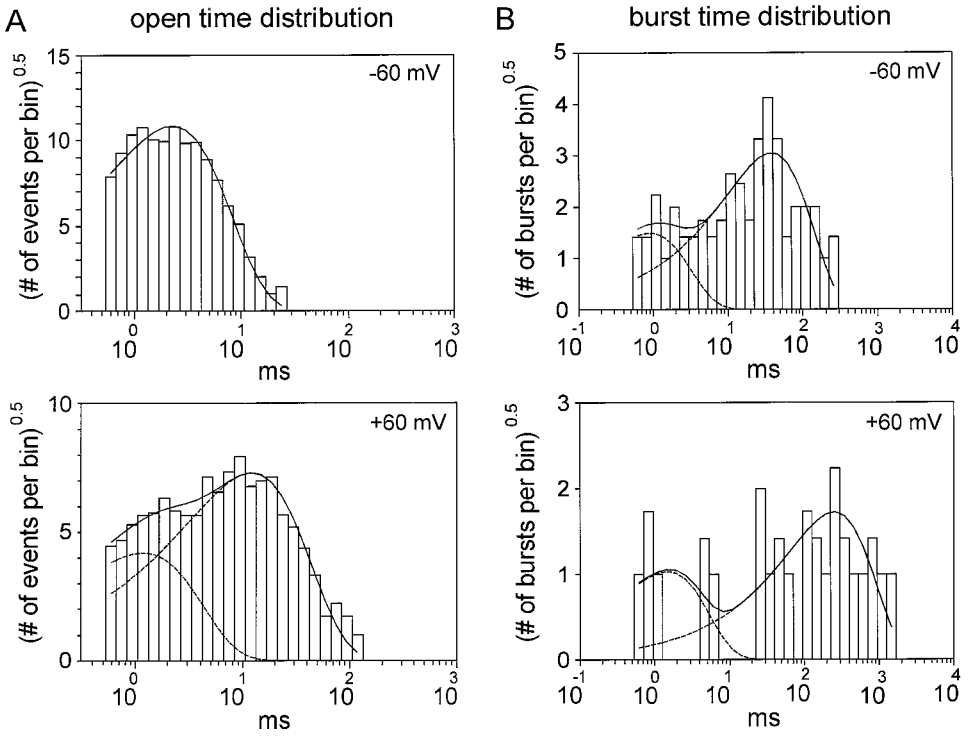

FIGURE 7 Analysis of 17-pS channel gating. (*A*) Open time distributions at −60 mV and +60 mV. The distribution at −60 mV was fitted to a single exponential function with a time constant of 2.2 ms. The open time distribution at +60 mV was fitted to two exponential functions with time constants τ_{O1} = 1.2 ms and τ_{O2} = 12.2 ms, and fractions of open events a_{O1} = 0.247 and a_{O2} = 0.753. (*B*) Distribution of burst lengths at −60 mV and +60 mV, for the same patch. The burst length distribution at −60 mV was fitted to the sum of two exponential functions: τ_{B1} = 0.9 ms, a_{B1} = 0.19; and τ_{B1} = 38.4 ms, a_{B1} = 0.81 (critical closed time: 6.8 ms). The distribution at +60 mV was also fitted to the sum of two exponential functions: τ_{B1} = 1.5 ms, a_{B1} = 0.27; and τ_{B1} = 251 ms, a_{B1} = 0.73 (critical closed time: 14.5 ms). Patch c5415.

17-pS channels at −60 mV was mostly due to transitions between bursts and long closed states.

Fig. 11 *B* shows that at least three Lorentzian functions are required to fit the power spectrum of a 6-pS channel. Table 2 summarizes results from three experiments. Like the 17-pS channel, the slowest Lorentzian component accounts for most of the total variance of 6-pS channels (76%). For the 6-pS channel, the Lorentzian components of the noise cannot be related directly to the time constants measured from channel dwell time distributions, because there were several open and closed times and at least two types of burst.

Whole-cell experiments

Leak currents at the whole-cell level were investigated using 110 mM Ba^{2+}. Gd^{3+}-sensitive Ba^{2+} currents (see Materials and Methods) were recorded at negative membrane potentials within the first 3 min after the whole-cell configuration was established, or after reaching a stable capacitative transient in the perforated patch-clamp configuration. Fig. 12 *A* shows whole-cell currents recorded in a perforated patch-clamp experiment before (0 Gd^{3+}) and after exposure to 50 μM Gd^{3+} (50 Gd^{3+}). The current-voltage relationship suggests that depolarization beyond −30 mV activates T- and L-type calcium currents, consistent with previous studies on A7r5 cells (Fish et al., 1988; McCarthy and Cohen, 1989; Obejero-Paz et al., 1990). In addition to blocking the T- and L-currents, Gd^{3+} blocked a small "leak" current at negative membrane potentials. The extrapolation of a line fitted to the difference current from −90 mV to −30 mV suggests that the leak current reverses at a positive membrane potential (Fig. 12 *A*, *inset*), in agreement with our single-channel data. The average current amplitudes at −60 mV with the perforated patch (−0.4 ± 0.3 pA/pF, range 0–1.0, n = 7) and classical whole-cell configurations (−0.7 ± 0.7 pA/pF, range 0–2.65, n = 22) were not significantly different. No difference was observed in the presence or absence of intracellular ATP dialysis (not shown). In three experiments, 2 μM nifedipine blocked 51 ± 3% of the L-current, with no effect on the whole-cell current at −60 mV or more negative membrane potentials, further evidence that the leak current does not result from L-channels.

The next set of experiments was designed to investigate whether the channel activity underlying the Gd^{3+}-sensitive Ba^{2+} currents shows spectral characteristics similar to those observed in single-channel experiments. Fig. 12 *B* shows an experiment using the classical whole-cell configuration, where 50 μM Gd^{3+} was added to block resting currents at −60 mV. Note that the decrease in inward current was paralleled by a decrease in current noise. The inset in Fig. 11 *C* shows the power spectra of whole-cell currents from this experiment, in the absence (0 Gd^{3+}) and presence (50 Gd^{3+}) of 50 μM Gd^{3+}. Fig. 11 *C* shows that the difference spectrum was well fitted to four Lorentzian functions, with the three larger time constants similar to the ones calculated from single-channel experiments (see Table 2). The shortest time constant was not well estimated because of bandwidth limitations.

The time constants of the two slowest components of the whole-cell spectra agreed well with the main (slowest) components of the single-channel spectra (Table 2). This allowed estimation of the number of open channels of each

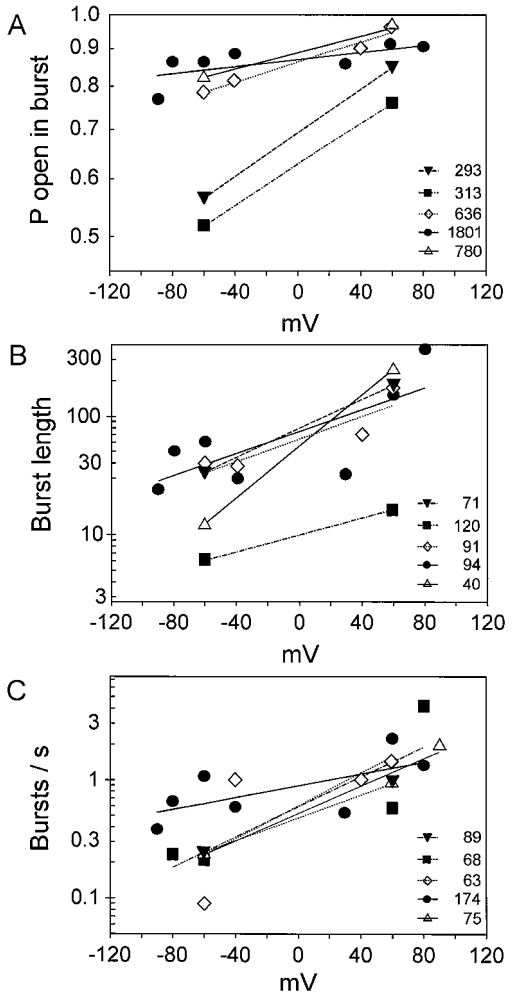

FIGURE 8 Effect of voltage on burst open probability (*A*), mean burst length (*B*), and burst rate (number of bursts per second) (*C*) of 17-pS channels. The mean burst length was calculated by fitting exponential functions to the burst time distribution, or by averaging the burst lengths when few bursts were observed. Numbers near the symbols in *A* and *B* indicate the change in membrane potential in millivolts necessary for an *e*-fold change.

type per cell, from the relative amplitudes of the corresponding Lorentzian components. From five whole-cell experiments, 111 ± 90 (range 25–241) 6-pS channels and 32 ± 28 (range 8–84) 17-pS channels were open at resting conditions. To assess whether the activity of these channels can account for the current recorded in whole-cell experiments, the expected current at −60 mV was calculated from

$$I = iNP_o \quad (6)$$

where i is the single-channel current, P_o is the open probability, and N is the number of channels. Using the i and P_o values from Table 1, the calculated resting current was −22 ± 18 pA, close to the measured whole cell current (−18 ± 9 pA). Taken together, these results support the notion that most of the resting whole-cell current in our experimental conditions results from the gating of the 6-pS and 17-pS channels.

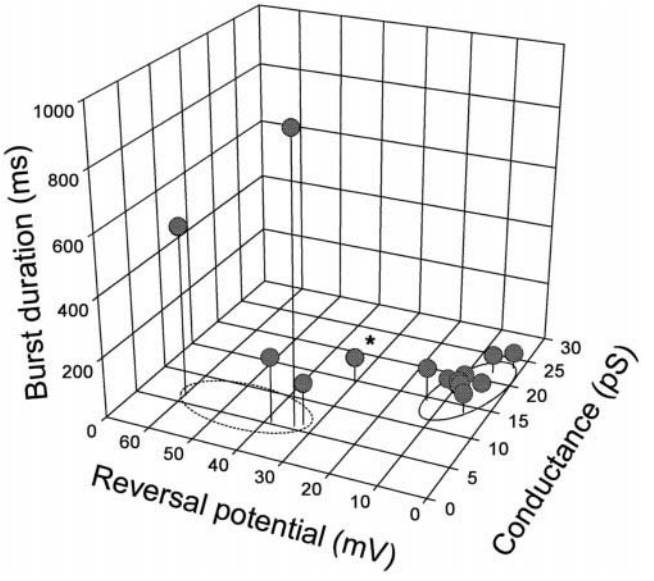

FIGURE 9 Criteria for identification of channel types. A three-dimensional graph of the relationships among mean burst duration, reversal potential, and slope conductance, for all experiments in 110 mM Ba^{2+}, where the three parameters were calculated. The data marked with an asterisk (patch d4o12) were from an unusual channel with a slope conductance of 15 pS (see text and Table 1). The burst length used in the figure is the larger time constant fitted to the burst length distributions of large and small channels.

DISCUSSION

Properties of Ca^{2+} leak channels in A7r5 cells

A7r5 cells have at least two different channels through which Ca^{2+} can enter the cell at resting membrane potentials (Table 1). The 6-pS channels are more selective for Ba^{2+} over K^+ than are the 17-pS channels. This selectivity may be even greater than the indicated values, because the extrapolated reversal potential of 6-pS channels may be underestimated, as no outward current was observed. Six-pS and 17-pS channels also differ in their conductance to Ca^{2+} and Ba^{2+}. The extrapolated reversal potential and slope conductance of 17 pS channels were comparable with Ca^{2+} or Ba^{2+}, but Ba^{2+} carried approximately three times more current through the small channel than did Ca^{2+}.

Because channel properties in Ca^{2+} and Ba^{2+} were characterized in different cell-attached patches, the interpretation of these results relies upon the assumption that the same channel type was studied under both ionic conditions. The similarity in conductance, gating properties, and frequency of observation of 17-pS channels in Ba^{2+} and Ca^{2+} is consistent with this possibility. The two small channels observed in Ca^{2+} resembled the 6-pS channels recorded with Ba^{2+} (Table 1), but the small single-channel currents with Ca^{2+} precluded a more conclusive kinetic analysis.

One interesting difference between small and large channels is the shape of the current-voltage relationship, as 6-pS channels pass no detectable outward current at positive potentials, whereas 17-pS channels have a linear current-

TABLE 1 Comparison of channels recorded with Ca^{2+} and Ba^{2+}

Channel type	Smaller channel (6 pS)		Larger channel (17 pS)		15 pS
Charge carrier	Ca^{2+}	Ba^{2+}	Ca^{2+}	Ba^{2+}	Ba^{2+}
Frequency*	2/27	9/142	4/27	10/142	1/142
Conductance (pS)	<6	6.0 ± 0.6 (8)	12.7 ± 1.6 (4)	17.1 ± 3.2 (10)	15
Single channel current (pA)	0.21 ± 0.05 (2)	0.61 ± 0.05 (4)	0.92 ± 0.13 (4)	1.15 ± 0.20 (10)	1.31
V_R (mV)	>41	41 ± 13 (8)	13 ± 5 (4)	7 ± 4 (10)	30
P_{Ba}/P_K	ND	27.6	4.1	2.9	12.8
Inward rectification	ND	Yes	ND	No	Yes
P_o	ND	0.32 ± 0.26 (3)	≤0.010 ± 0.005 (3)[#]	0.005 ± 0.005 (5)	0.092
Open time[§] (ms)	ND	0.8 ± 0.2 (4)	1.4 ± 0.3 (3)	2.1 ± 1.4 (9)	1.4
Fraction of open events[§]	ND	0.43 ± 0.05 (4)	0.79 ± 0.19 (3)	0.85 ± 0.21 (9)	0.55
Burst length (ms)	ND	τ_1 = 27 ± 9 τ_2 = 464 ± 317 (4)	37 ± 14 (3)	5 ± 39 (9)	τ_1 = 12 τ_2 = 84
P_o in burst	ND	0.84 ± 0.10 (4)	0.48 ± 0.28 (3)	0.74 ± 0.14 (9)	0.66

Summary of the permeation and gating properties of the channels characterized in this work. Where appropriate, values are mean ± SD with the number of patches in parentheses. ND, Not determined. The single-channel current, P_o, open times, and burst parameters were measured at −60 mV.

* The number of patches with this type of channel/the number of patches examined.

[#] Because the number of channels per patch in these experiments is unknown, the value given is NP_o, and the ≤ symbol indicates that P_o may be overestimated.

[§] Mean open times and fraction of open events for the exponential component most frequent in each experimental condition.

voltage relationship. The inward rectification of the 6-pS channel could be accounted for by several mechanisms: 1) Inward rectification could be of the Goldman-type resulting from the Ba^{2+} gradient. This would be consistent with the high selectivity of that channel for Ba^{2+} over K^+. 2) Rectification could also result from an intrinsic voltage-dependent gating mechanism with long-lived closed states at positive membrane potentials. However, the apparently instantaneous inward currents upon repolarization (Fig. 2 *C*) would require extremely fast channel opening at negative potentials. 3) Inward rectification could also result from block by a positively charged intracellular molecule, driven into the channel by depolarization.

Six-pS and 17-pS channels have complex kinetics with multiple open and closed states. Both channels gated in bursts of activity separated by long closures lasting up to several minutes, often producing clusters of bursts. However, the two channels show different kinetics. Seventeen-pS channels showed one predominant type of burst, whereas 6-pS channels showed short bursts with low P_o and long bursts with high P_o. The 17-pS channel, but not the 6-pS channels, showed voltage-dependent gating.

Comparison to Ca^{2+} leak channels in other cells

Leak channels with complex kinetics and voltage dependence have been described for other cells (Coyne et al., 1987; Preston et al., 1992; Coulombe et al., 1989; Chesnoy-Marchais, 1985; Kuno et al., 1986; Franco and Lansman, 1990a; Rosenberg et al., 1988; Fong et al., 1990). In vascular smooth muscle cells from rabbit ear artery, Benham and Tsien (1987) described a channel with a slope conductance of 16 pS and an extrapolated reversal potential close to +10 mV in isotonic Ba^{2+}, similar to the 17-pS channel in our experiments. The 17-pS channel of A7r5 cells is also similar in conductance and kinetics to the leak channel described in developing skeletal muscle fibers (Franco and Lansman, 1990b), where burst duration also increased at more positive potentials and at least three exponential functions were required to fit the closed time distribution. The permeation properties of those channels are similar, with slope conductance ranging from 16 to 24 pS, a reversal potential near +20 mV, and a calculated P_{Ba}/P_K ratio close to 2 (Franco and Lansman, 1990b). Gating of the 19-pS channel in skeletal muscle was stretch-dependent, a property that we have not tested in our experiments.

The 17-pS channel shares some similarities with the channel encoded by the transient receptor potential-like (TRPL) gene involved in phototransduction in *Drosophila*. This channel is slightly selective for divalent cations (P_{Ca}/P_{Cs} = 2.6) and shows voltage-dependent gating, with the open probability increasing at positive membrane potentials (Hardie et al., 1997). Interestingly, expression of TRPL in Sf9 cells produced a constitutive active calcium entry pathway (Hu et al., 1994).

The 6-pS channel may have even more physiological relevance in cellular Ca^{2+} homeostasis, as it is more likely to select for Ca^{2+} over monovalent cations under physiological ionic conditions. This channel is similar in conductance, voltage independence of channel gating, and some kinetic properties, to a lectin-activated channel open at resting conditions in lymphocytes (Kuno et al., 1986). The 6-pS channel shares some kinetic similarity with the channel activated by depletion of intracellular Ca^{2+} stores in A431 cells, which may open rarely at resting conditions (Luckhoff and Clapham, 1994). However, the A431 channel had slope conductances of 16 pS with 160 mM Ba^{2+} and 2 pS with 200 mM Ca^{2+}. Another channel that is activated by depletion of intracellular stores and shows a finite probability of being open in resting conditions was demonstrated in bovine aortic endothelial cells (Vaca and Kunze, 1994). In 10 mM Ca^{2+} this channel shows a slope conductance of

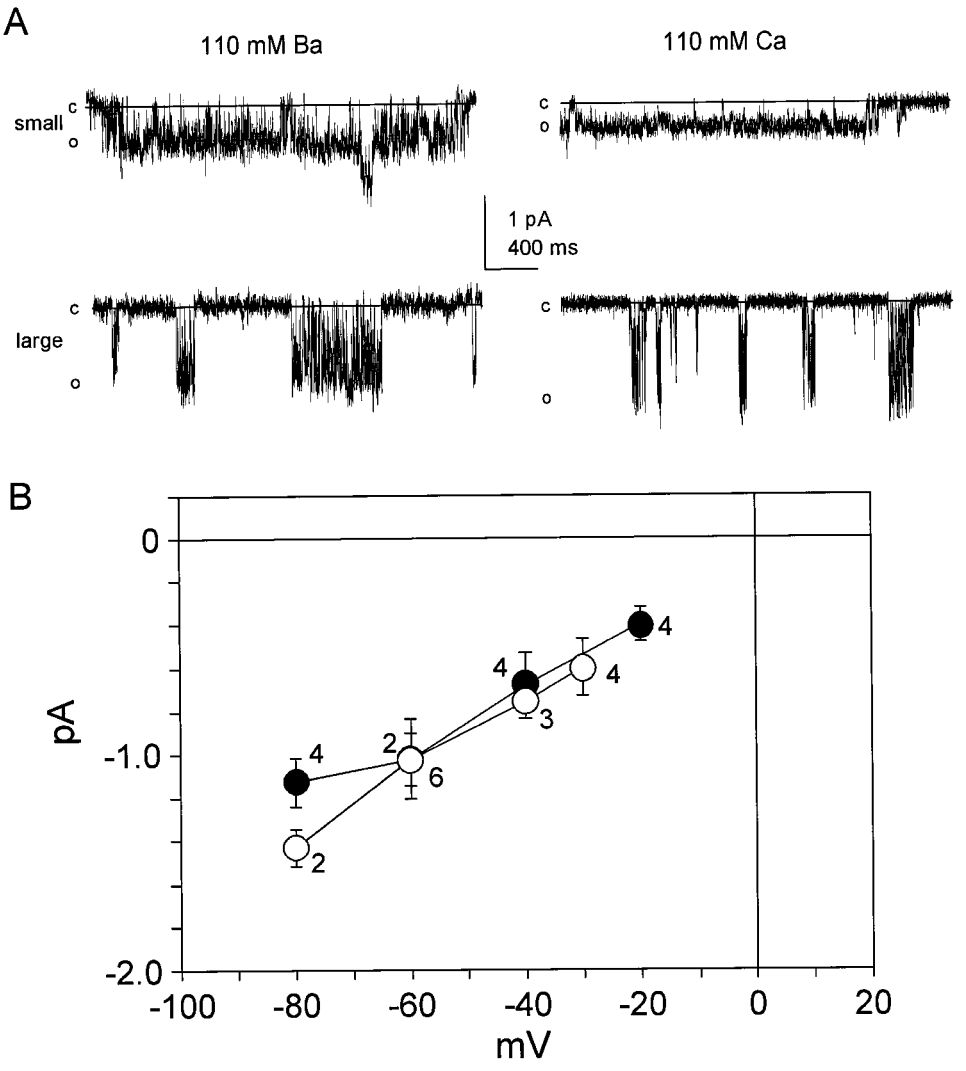

FIGURE 10 Comparison of channels with Ca^{2+} and Ba^{2+}. (*A*) Burst activity of small and large channels in the presence of 110 mM Ba^{2+} and 110 mM Ca^{2+}. (*B*) Current-voltage relationships at negative membrane potentials, from experiments in 110 mM Ba^{2+} (○) and 110 mM Ca^{2+} (●). Values are mean ± SD, with the number of experiments indicated near each symbol.

11 pS, a reversal potential of +30 mV, and strong inward rectification.

Basal Ca^{2+} entry in A7r5 cells

The presence of at least two calcium channels in resting A7r5 cells is consistent with Fura 2 experiments showing that these cells express multiple pathways for Ca^{2+}, Ba^{2+}, and Mn^{2+} entry (Hughes and Schachter, 1994). The amount of Ca^{2+} influx expected from our 6-pS and 17-pS channels is also in general agreement with ^{45}Ca flux measurements (Fayazi et al., 1996). Assuming that monovalent and divalent cations permeate independently following a Goldman-Hodgkin-Katz relationship, and that the permeability ratios calculated in isotonic Ba^{2+} apply to physiological Ca^{2+}, we calculate a single-channel current of −0.06 pA for 6-pS channels at −60 mV. The current carried by Ca^{2+} in this condition would be −0.03 pA. For 17-pS channels, the estimated single-channel current was −0.45 pA, with −0.06 pA carried by Ca^{2+}. From these values, and our estimates of the number of open 6-pS channels (111) and 17-pS channels (32), we estimate a total Ca^{2+} entry of 0.36 fmol min^{-1}. This is six times larger than the value from ^{45}Ca influx (0.06 fmol min^{-1}; Fayazi et al., 1996). Part of the difference may be accounted for by an inhibition by Mg^{2+}, as the tracer experiments were carried out in the presence of 1 mM Mg^{2+}, and we find that extracellular Mg^{2+} significantly decreases resting currents in 110 mM Ba^{2+} (data not shown).

One possible role for calcium channel activity at resting membrane potentials is refilling of intracellular stores after Ca^{2+} mobilization by vascular agonists (Hoth and Penner, 1992; Luckhoff and Clapham, 1994; Hughes and Schachter, 1994; Van Renterghem and Lazdunski, 1994). This capacitative calcium entry mechanism has been shown in A7r5 cells and the related smooth muscle cell line A10 (Missiaen et al., 1990; Byron and Taylor, 1995; Xuan et al., 1992; but see Hughes and Schachter, 1994). Even in the absence of agonist, the finite open probability of leak channels could help maintain stable intracellular Ca^{2+} levels (Missiaen et al., 1993; Fayazi et al., 1996). As noted above, the channels reported here have some similarities to channels involved in

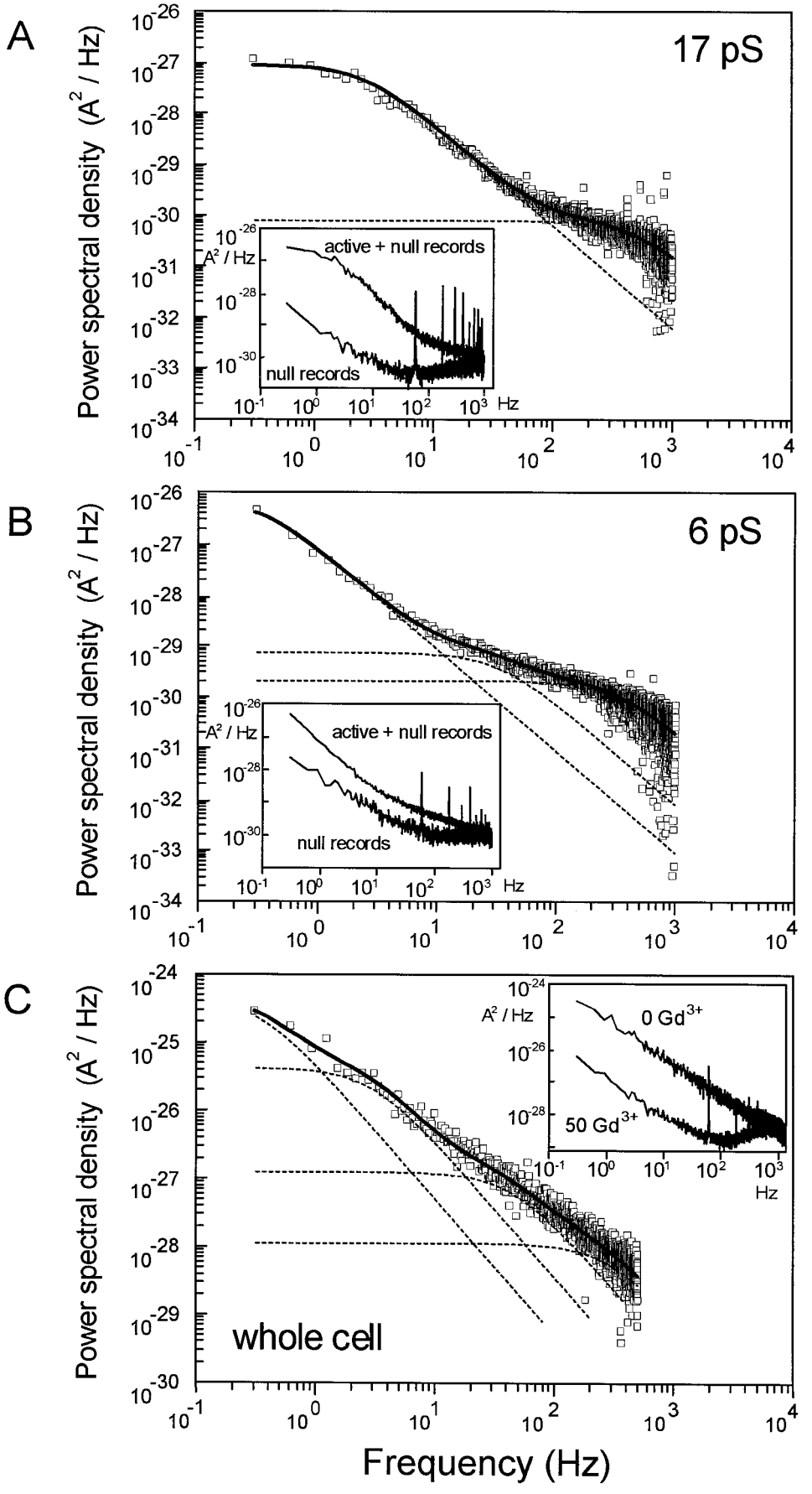

FIGURE 11 Power spectra from single-channel and whole-cell records. (*A*) Power spectrum of a 17-pS channel obtained by subtraction of spectra shown in the inset. The spectrum was fitted to the sum of two Lorentzian functions: f_{c1} = 2.6 Hz, f_{c2} = 476 Hz; S_1 (0) = 9.1 A^2/(Hz 10^{28}), S_2 (0) = 0.008 A^2/(Hz 10^{28}). Patch d6720. (*B*) Power spectrum of a 6-pS channel fitted to three Lorentzian functions: f_{c1} = 0.34 Hz, f_{c2} = 33 Hz, and f_{c3} = 316 Hz; S_1 (0) = 73 A^2/(Hz 10^{28}), S_2 (0) = 0.07 A^2/(Hz 10^{28}), and S_3 (0) = 0.02 A^2/(Hz 10^{28}). Patch b3o01. (*C*) Power spectrum of Gd^{3+}-sensitive currents from the experiment in Fig. 12 *B*. Power spectra of whole-cell currents before and after blocking with 50 μM Gd^{3+} are depicted in the inset. The difference current was fitted to the sum of four Lorentzian functions: f_{c1} = 0.33 Hz, f_{c2} = 3.0 Hz, f_{c3} = 44 Hz, and f_{c3} = 284 Hz; S_1 (0) = 4490 A^2/(Hz 10^{28}), S_2 (0) = 419 A^2/(Hz 10^{28}), S_3 (0) = 12 A^2/(Hz 10^{28}), and S_4 (0) = 1.1 A^2/(Hz 10^{28}). Single Lorentzian functions and the sum of multiple Lorentzians are depicted as dashed and solid lines, respectively.

TABLE 2 Spectral characteristics of single-channel and whole-cell currents

	Time constants (ms)				*n*
6 pS	433 ± 56		4.5 ± 0.6	0.4 ± 0.1	3
17 pS		59 ± 12		0.4 ± 0.03	5
Whole cell	435 ± 39	61 ± 9	5.8 ± 1.4	0.7 ± 0.2	5
	Amplitude at zero frequency (A^2/(Hz 10^{28}))				
6 pS	69 ± 24		0.082 ± 0.038	0.013 ± 0.006	3
17 pS		16 ± 13		0.019 ± 0.013	5
Whole cell	7600 ± 6200	510 ± 450	32 ± 25	3.3 ± 2.4	5

Power spectra were calculated from single-channel records showing either 6-pS or 17-pS activity, and from whole-cell experiments. Lorentzian components with similar time constants in single-channel and whole-cell recordings were aligned for clarity. The right column indicates the number of experiments analyzed.

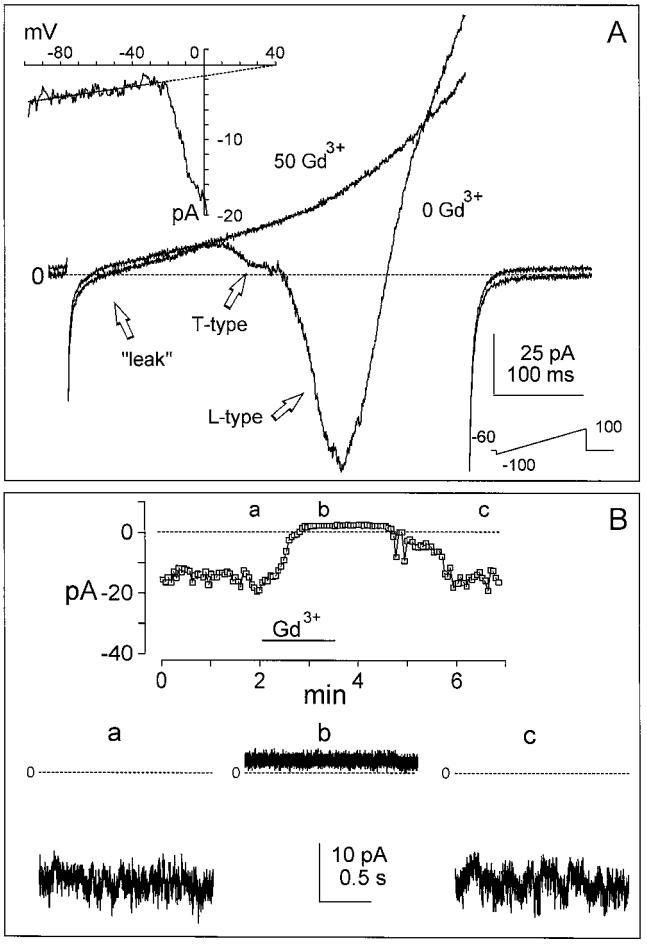

FIGURE 12 Whole-cell currents in isotonic Ba^{2+}. (*A*) Currents during voltage ramps from −100 mV to +100 mV before (0 Gd^{3+}) and after exposure to 50 mM Gd^{3+} (50 Gd^{3+}) in a perforated patch-clamp experiment. In each condition four currents were averaged. *Inset*: Difference current ±Gd^{3+}, from −100 to 0 mV. The straight line was fitted from −90 to −30 mV. Cell a7701, whole-cell capacitance = 27.4 pF. (*B*) Currents at −60 mV with isotonic Ba^{2+} in the classical whole-cell configuration. Each point represents the average of 16,384 samples recorded at 5000 Hz. Sample records taken at the indicated times are shown below. Cell c7908, whole-cell capacitance = 16 pF.

capacitative Ca^{2+} entry. However, it is not likely that the channel activity observed in our experimental conditions resulted from the depletion of intracellular Ca^{2+} stores. Although the cells were bathed in a low Ca^{2+} solution for the single-channel recordings, A7r5 cells exposed to low Ca^{2+} show only small decreases in subsarcolemmal and cytosolic Ca^{2+} concentrations after 10 min (26% and 13% of the resting Ca^{2+}, respectively; Himpens et al., 1994). This suggests that changes in Ca^{2+} content of intracellular stores would develop slowly, whereas background channel activity in some instances was noted at the beginning of the experiment. In addition, we observed resting currents with Ba^{2+} in perforated patch recordings, where no depletion of intracellular calcium stores should occur.

In preliminary experiments, we have observed resting Gd^{3+}-sensitive currents in primary cultured aortic cells, suggesting that the leak channel activity of A7r5 cells is shared by other smooth muscle cells (not shown).

Leak channels may not be the only pathways for calcium entry at resting membrane potentials in physiological Ca^{2+}. Evidence for L-type calcium channel activity under resting conditions has been presented for smooth muscle cells from coronary (Ganitkevich and Isenberg, 1990) and posterior cerebral (Rubart et al., 1996) arteries. Hayashi et al. (1991) reported that 40% of resting Ca^{2+} entry in A7r5 cells is sensitive to DHPs, although no DHP-sensitive resting Ca^{2+} entry was found by Himpens et al. (1994) in A7r5 cells or by Orlov et al. (1993) in cultured aortal smooth muscle cells. Voltage-dependent calcium entry through L-type calcium channels occurs in a "voltage window," where at steady state some channels are not inactivated, and have a low but finite probability of being open (Imaizumi et al., 1989; Fleischmann et al., 1994). We have not investigated L-channel channel activity in steady recordings at negative membrane potentials in single-channel experiments. However, the channels observed in this study are not L-channels, because 1) L-channels are more strongly voltage-dependent, and show rare brief openings rather than bursts at strongly negative voltages (Ganitkevich and Isenberg, 1990), and 2) L-channels have a slope conductance of 25 pS (Obejero-Paz et al., 1993) with predicted single-channel current of −2.7 pA at −60 mV, twice the current carried by the 17 pS channel (see Table 1).

There is evidence for the presence of T-type calcium channels in A7r5 cells (Fish et al., 1988; McCarthy and Cohen, 1989) and native vascular smooth muscle cells (Benham and Tsien, 1987; Ganitkevich and Isenberg, 1990; Ohya et al., 1993; Wilde et al., 1994; McDonald et al., 1994). However, we can exclude the possibility that the channels observed here were T-type calcium channels, which have a slope conductance of 12 pS and gate in short bursts (Chen and Hess, 1990). Moreover, our whole-cell experiments show that in isotonic Ba^{2+} only a very small

fraction of L-type and T-type calcium channels would be open at −60 mV (see Fig. 12 *A*). Nonetheless, a small fraction of L- and T-channels could be open at resting physiological Ca^{2+} because of the shift of the activation curve toward more negative values (Rubart et al., 1996). Further experiments will be necessary to evaluate the relative contribution of L-, T-, and leakage channels to calcium entry at resting membrane potentials, especially in native vascular smooth muscle cells under physiological conditions.

In conclusion, our results define two possible pathways for calcium entry at resting membrane potentials in unstimulated A7r5 cells: a highly selective 6-pS channel that does not pass detectable outward current, and a weakly selective 17-pS channel with moderately voltage-dependent gating. These channels can account for the current recorded at hyperpolarized membrane potentials in whole-cell experiments.

We thank Dr. Keith S. Elmslie for helpful discussions during the development of this work and Carol Bertrand for helpful discussions on noise analysis and the calculation of the corner frequency for whole-cell experiments. We also thank Dr. Marcelo Auslender for helping in some experiments.

This work was supported by National Institute of Health grant HL 41618 to AS, and an American Heart Association (Northeast Ohio Affiliate) postdoctoral fellowship to CAO-P. SWJ was an Established Investigator of the American Heart Association.

REFERENCES

Benham, C. D., and R. W. Tsien. 1987. Calcium-permeable channels in vascular smooth muscle: voltage-activated, receptor-operated, and leak channels. *Soc. Gen. Physiol. Ser.* 42:45–64.

Byron, K. L., and C. W. Taylor. 1995. Vasopressin stimulation of Ca^{2+} mobilization, two bivalent cation entry pathways and Ca^{2+} efflux in A7r5 rat smooth muscle cells. *J. Physiol. (Lond).* 485:455–468.

Chen, C., and P. Hess. 1990. Mechanism of gating of T-type calcium channels. *J. Gen. Physiol.* 96:603–630.

Chesnoy-Marchais, D. 1985. Kinetic properties and selectivity of calcium permeable single channels in *Aplysia* neurones. *J. Physiol. (Lond).* 367:457–488.

Colquhoun, D., and A. G. Hawkes. 1995. The principles of the stochastic interpretation of ion-channel mechanisms. *In* Single-Channel Recording, 2nd Ed. B. Sakmann and E. Neher, editors. Plenum Press, New York. 397–482.

Colquhoun, D., and F. J. Sigworth. 1983. Fitting and statistical analysis of single channel records. *In* Single-Channel Recording. B. Sakmann and E. Neher, editors. Plenum Press, New York. 191–263.

Coulombe, A., I. A. Lefevre, I. Baro, and E. Coraboeuf. 1989. Barium- and calcium-permeable channels open at negative membrane potentials in rat ventricular myocytes. *J. Membr. Biol.* 111:57–67.

Coyne, M. D., D. Dagan, and I. B. Levitan. 1987. Calcium and barium permeable channels from *Aplysia* nervous system reconstituted in lipid bilayers. *J. Membr. Biol.* 97:205–213.

Fayazi, A. H., S. A. Lapidot, B. K. Huang, R. W. Tucker, and R. D. Phair. 1996. Resolution of the basal plasma membrane calcium flux in vascular smooth muscle cells. *Am. J. Physiol.* 270:H1972–H1978.

Fish, R. D., G. Sperti, W. S. Colucci, and D. E. Clapham. 1988. Phorbol ester increases the dihydropyridine-sensitive calcium conductance in a vascular smooth muscle cell line. *Circ. Res.* 62:1049–1054.

Fleischmann, B. K., R. K. Murray, and M. Kotlikoff. 1994. Voltage window for sustained elevation of cytosolic calcium in smooth muscle cells. *Proc. Natl. Acad. Sci. USA.* 91:11914–11918.

Fong, P., P. R. Turner, W. F. Dennetclaw, and R. A. Steinhardt. 1990. Increased activity of calcium leak channels in myotubes of Duchenne human and mdx mouse origin. *Science.* 50:673–676.

Franco, A., Jr., and J. B. Lansman. 1990a. Calcium entry through stretch inactivated ion channels in mdx myotubes. *Nature.* 344:670–673.

Franco, A., Jr., and J. B. Lansman. 1990b. Stretch-sensitive channels in developing muscle cells from a mouse cell line. *J. Physiol. (Lond.).* 427:361–380.

Franco, A., Jr., B. D. Winegar, and J. B. Lansman. 1991. Open channel block by gadolinium ion of the stretch-inactivated ion channel in mdx myotubes. *Biophys. J.* 59:1164–1170.

Ganitkevich, V. Y., and G. Isenberg. 1990. Contribution of two types of calcium channels to membrane conductance of single myocytes from guinea-pig coronary artery. *J. Physiol. (Lond.).* 426:19–42.

Goldbeter, A., G. Dupont, and M. J. Berridge. 1990. Minimal model for signal-induced Ca^{2+} oscillations and for their frequency encoding through protein phosphorylation. *Proc. Natl. Acad. Sci. USA.* 87: 1461–1465.

Hardie, R. C., H. Reuss, S. J. Lansdell, and N. S. Millar. 1997. Functional equivalence of native light-sensitive channels in the *Drosophila* trp^{301} mutant and TRPL cation channels expressed in a stably transfected *Drosophila* cell line. *Cell Calcium.* 21:431–440.

Hayashi, T., T. Nakai, and S. Miyabo. 1991. Glucocorticoids increase Ca^{2+} uptake and [^{3}H]dihydropyridine binding in A7r5 vascular smooth muscle cells. *Am. J. Physiol.* 261:C106–C114.

Himpens, B., H. De Smedt, and R. Casteels. 1994. Subcellular Ca^{2+}-gradients in A7r5 vascular smooth muscle. *Cell Calcium.* 15:55–65.

Horn, R. 1987. Statistical methods for model discrimination. Applications to gating kinetics and permeation of the acetylcholine receptor channel. *Biophys. J.* 51:255–263.

Hoth, M., and R. Penner. 1992. Depletion of intracellular calcium stores activates a calcium current in mast cells. *Nature.* 355:353–356.

Hu, Y., L. Vaca, X. Zhu, L. Birnbaumer, D. L. Kunze, and W. P. Schilling. 1994. Appearance of a novel Ca^{2+} influx pathway in SF9 insect cells following expression of the transient receptor potential-like (trpl) protein of *Drosophila*. *Biochem. Biophys. Res. Commun.* 201:1050–1056.

Hughes, A. D., and M. Schachter. 1994. Multiple pathways for entry of calcium and other divalent cations in a vascular smooth muscle cell line (A7r5). *Cell Calcium.* 15:317–330.

Imaizumi, Y., K. Muraki, M. Takeda, and M. Watanabe. 1989. Measurement and simulation of noninactivating Ca current in smooth muscle cells. *Am. J. Physiol.* 256:C880–C885.

Jackson, M. B., B. S. Wong, C. E. Morris, and H. Lecar. 1983. Successive openings of the same acetylcholine receptor channel are correlated in open time. *Biophys. J.* 42:109–114.

Karaki, H., H. Ozaki, M. Hori, M. Mitsui-Saito, K. Amano, K. Harada, S. Miyamoto, H. Nakazawa, K. Won, and K. Sato. 1997. Calcium movements, distribution, and functions in smooth muscle. *Pharmacol. Rev.* 49:157–230.

Kargacin, G., and F. S. Fay. 1991. Ca^{2+} movement in smooth muscle cells studied with one- and two-dimensional diffusion models. *Biophys. J.* 60:1088–1100.

Kimes, B. W., and B. L. Brandt. 1976. Characterization of two putative smooth muscle cells lines from rat thoracic aorta. *Exp. Cell. Res.* 98:349–366.

Kuno, M., J. Goronzy, C. M. Weyand, and P. Gardner. 1986. Single-channel and whole-cell recordings of mitogen-regulated inward currents in human cloned helper T lymphocytes. *Nature.* 323:269–273.

Lapidot, S. A., B. K. Huang, A. Fayazi, L. N. Russek, S. A. Strickberger, A. E. Brooks, and R. D. Phair. 1996. Mechanisms for Ca signaling in vascular smooth muscle: resolved from ^{45}Ca uptake and efflux experiments. *Cell Calcium.* 19:167–184.

Lewis, C. A. 1979. Ion-concentration dependence of the reversal potential and the single channel conductance of ion channels at the frog neuromuscular junction. *J. Physiol. (Lond.).* 186:417–445.

Loutzenhiser, R., P. Leyten, K. Saida, and C. van Breemen. 1984. Calcium compartments and mobilization during contraction of smooth muscle. *In* Calcium and Contractility, Smooth Muscle. A. K. Grover and E. E. Daniel, editors. Humana Press, Clifton, NJ. 62–64.

Luckhoff, A., and D. E. Clapham. 1994. Calcium channels activated by depletion of internal calcium stores in A431 cells. *Biophys. J.* 67: 177–182.

Marks, T. N., G. R. Dubyak, and S. W. Jones. 1990. Calcium currents in the A7r5 smooth muscle-derived cell line. *Pflügers Arch.* 417:433–439.

McCarthy, R. T., and C. J. Cohen. 1989. Nimodipine block of calcium channels in rat vascular smooth muscle cell lines. Exceptionally high-affinity binding in A7r5 and A10 cells. *J. Gen. Physiol.* 94:669–692.

McDonald, T. F., S. Pelzer, W. Trautwein, and D. J. Pelzer. 1994. Regulation and modulation of calcium channels in cardiac, skeletal, and smooth muscle cells. *Physiol. Rev.* 74:365–507.

Missiaen, L., I. Declerck, G. Droogmans, L. Plessers, H. De Smedt, L. Raeymaekers, and R. Casteels. 1990. Agonist-dependent Ca^{2+} and Mn^{2+} entry dependent on state of filling of Ca^{2+} stores in aortic smooth muscle cells of the rat. *J. Physiol. (Lond.).* 427:171–186.

Missiaen, L., J. B. Parys, H. De-Smedt, and R. Casteels. 1993. Ins(1,4,5)P3 and glutathione increase the passive Ca^{2+} leak in permeabilized A7r5 cells. *Biochem. Biophys. Res. Commun.* 193:6–12.

Obejero-Paz, C. A., M. Auslender, and A. Scarpa. 1994. Calcium currents at resting membrane potential in the A7r5 smooth muscle-derived cell line. *Biophys. J.* 66:a81.

Obejero-Paz, C. A., S. W. Jones, and A. Scarpa. 1997. "Leak" calcium channels in A7r5 vascular smooth muscle cells. *Biophys. J.* 72:A355.

Obejero-Paz, C. A., S. W. Jones, and A. Scarpa. 1998. Noise analysis of resting whole cell currents reveals the gating of multiple calcium channels in the A7r5 smooth muscle derived cell line. *Biophys. J.* 74:A103.

Obejero-Paz, C. A., M. Lakshmanan, S. W. Jones, and A. Scarpa. 1993. Effects of dexamethasone on L-type calcium currents in the A7r5 smooth muscle-derived cell line. *FEBS Lett.* 333:73–77.

Obejero-Paz, C., T. Marks, S. Jones, G. Dubyak, and A. Scarpa. 1990. Kinetics of activation of L-type calcium channels in the A7r5 smooth muscle cell line. *Biophys. J.* 57:522a.

Obejero-Paz, C. A., and A. Scarpa. 1992. Leak calcium channels in the A7r5 vascular smooth muscle cell line. *Biophys. J.* 61:a247.

Ohya, T., I. Abe, K. Fujii, Y. Takata, and M. Fujishima. 1993. Voltage-dependent Ca^{2+} channels in resistance arteries from spontaneously hypertensive rats. *Circ. Res.* 73:1090–1099.

Orallo, F. 1996. Regulation of cytosolic calcium levels in vascular smooth muscle. *Pharmacol. Ther.* 69:153–171.

Orlov, S., T. J. Resink, J. Bernhardt, F. Ferracin, and F. R. Buhler. 1993. Vascular smooth muscle cell calcium fluxes. Regulation by angiotensin II and lipoproteins. *Hypertension.* 21:195–203.

Patlak, J. B. 1993. Measuring kinetics of complex single ion channel data using mean-variance histograms. *Biophys. J.* 65:29–42.

Pitzer, K. S., and G. Mayorga. 1973. Thermodynamics of electrolytes. II. Activity and osmotic coeficients for strong electrolytes with one or both ions univalent. *J. Phys. Chem.* 77:2300–2308.

Press, W. H., S. A. Teukolsky, W. T. Vetterling, and B. P. Flannery. 1992. Numerical Recipes in Fortran 77. The Art of Scientific Computing. Cambridge University Press, New York.

Preston, R. R., Y. Saimi, and C. Kung. 1992. Calcium current activated upon hyperpolarization of *Paramecium tetraurelia. J. Gen. Physiol.* 100:233–251.

Rae, J., K. Cooper, G. Gates, and M. Watsky. 1991. Low access resistance perforated patch recording using amphotericin B. *J. Neurosci. Methods.* 37:15–26.

Rosenberg, R. L., P. Hess, and R. W. Tsien. 1988. Cardiac calcium channels in planar lipid bilayers. L-type channels and calcium-permeable channels open at negative membrane potentials. *J. Gen. Physiol.* 92:27–54.

Rubart, M., J. B. Patlak, and M. T. Nelson. 1996. Ca^{2+} currents in cerebral artery smooth muscle cells of rat at physiological Ca^{2+} concentrations. *J. Gen. Physiol.* 107:459–472.

Shatkay, A. 1968. Individual activity of calcium ions in pure solutions of $CaCl_2$ and in mixtures. *Biophys. J.* 8:912–919.

Sigworth, F. J., and S. M. Sine. 1987. Data transformations from improved display and fitting of single-channel dwell time histograms. *Biophys. J.* 52:1047–1054.

Tsien, R. W., and R. Y. Tsien. 1990. Calcium channels, stores, and oscillations. *Annu. Rev. Cell. Biol.* 6:715–760.

Vaca, L., and D. L. Kunze. 1994. Depletion of intracellular Ca^{2+} stores activates a Ca^{2+}-selective channel in vascular endothelium. *Am. J. Physiol.* 267:C920–C925.

Van Breemen, C., C. Cauvin, A. Johns, P. Leijten, and H. Yamamoto. 1986. Ca^{2+} regulation of vascular smooth muscle. *Fed. Proc.* 45: 2746–2751.

Van Renterghem, C., and M. Lazdunski. 1994. Identification of the Ca^{2+} current activated by vasoconstrictors in vascular smooth muscle cells. *Pflügers Arch.* 429:1–6.

Wilde, D. W., P. B. Furspan, and J. F. Szocik. 1994. Calcium current in smooth muscle cells from normotensive and genetically hypertensive rats. *Hypertension.* 24:739–746.

Wong, A. Y. K., and G. A. Klassen. 1993. A model of calcium regulation in smooth muscle cell. *Cell Calcium.* 14:227–243.

Xuan, Y., O. Wang, and A. R. Whorton. 1992. Thapsigargin stimulates Ca^{2+} entry in vascular smooth muscle cells: nicardipine-sensitive and -insensitive pathways. *Am. J. Physiol.* 262:C1258–C1265.